Strain Lattice Imprinting in Graphene by C_{60} Intercalation at the Graphene/Cu Interface

E. Monazami,[†] L. Bignardi,[‡] P. Rudolf,[‡] and P. Reinke*,[†]

[†]University of Virginia, 395 McCormick Road, P.O. Box 400745, Charlottesville, Virginia 22904-4745, United States
[‡]Zernike Institute for Advanced Materials, University of Groningen, Nijenborgh 4, NL-9747AG Groningen, The Netherlands

ABSTRACT: Intercalation of C_{60} molecules at the graphene-substrate interface by annealing leads to amorphous and crystalline structures. A comparison of topography and electronic structure with wrinkles and moiré patterns confirms intercalation. The intercalated molecules imprint a local strain/deformation on the graphene layer whose magnitude is controlled by the intermolecular distance. The crystalline intercalated structure exhibits a superlattice peak in the local density of states. This work provides control of local strain in graphene.

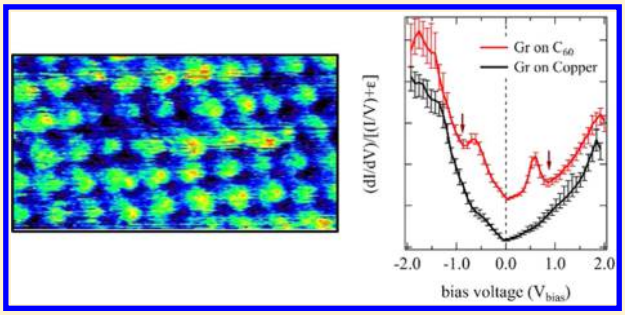

KEYWORDS: *graphene, fullerene, intercalation, superlattice, scanning tunneling microscopy, scanning tunneling spectroscopy*

The unique physical, chemical and mechanical properties of graphene have attracted unprecedented attention and have lead in the past decade to the development and augmentation of a wide range of applications. These include electronic devices that make use of the unique Dirac-type band structure at the K-point.[1−3] Graphene's two-dimensional structure allows modulation of its properties through the interaction with the substrate or by surface adsorbates.[4−17] This approach is highly versatile and can modify graphene's properties while simultaneously conserving the Dirac cone. The challenge is to find suitable pathways to achieve the desired graphene modulation. We focus in our work on the implementation of well-defined strain fields[18,19] by intercalation of C_{60} molecules at the graphene−Cu interface. This creates highly localized strain states introduced in the graphene layer by the buried molecules, whose spatial distribution can be controlled by the intercalation process.

The main strategies to modify graphene and achieve new functionalities are currently (i) doping by intercalation,[13,20,21] (ii) superposition of a periodic potential by superlattices,[22,23] (iii) introduction of local strain,[24] (iv) electrostatic modulation,[9] (v) chemical functionalization, (vi) ionic-liquid induced doping,[25] and (vii) nanoscale patterning to form nanoribbons and achieve control of the edge states and electronic confinement.[26] Our study combines strategies i to iii and expands the available intercalation strategies by use of molecular intercalants. Intercalation is a well-known method to achieve charge doping in layered van der Waals bonded materials such as graphite or h-BN. For graphene, the intercalation of alkali metals at the graphene−SiC interface has been used to achieve charge doping as a means to introduce a bandgap.[15] On the other hand, graphene can be electronically decoupled from a metal substrate by the intercalation of weakly interacting metal atoms nearly restoring the Dirac cone.[21] The intercalation of Pb islands at the graphene−Ir(111) interface introduces a significant enhancement in the spin−orbit splitting for charge carriers residing in graphene which potentially leads to novel physical phenomena.[27]

The introduction of localized strain modifies the charge transport in graphene through a change in the on-site energies of the p_z orbitals of adjacent carbon atoms and in turn influences the hopping parameter. The impact of strain on graphene's electronic structure has been discussed in numerous theoretical studies[9,18,23,24,28−33] and has recently been described in the framework of a pseudomagnetic field, whose strength depends on the magnitude and symmetry of the strain field.[19,34] The experimental challenges in creating well-defined and stable strain states are considerable and have been approached by substrate patterning with trenches, electrostatically driven deformation, thermally induced ripple structures,[35] and by gas intercalation to form nanobubbles.[19]

The work on C_{60} intercalation at the graphene−Cu interface presented in this study establishes a new strategy to control local strain and achieves at the same time positional control of the strained regions in amorphous and crystalline structures. Scanning tunneling microscopy (STM) and spectroscopy (STS) are used to study the electronic and topographic signatures of the intercalated material. The intercalation of C_{60} at the graphene−Cu interface was achieved for a polycrystalline Cu substrate by a thermally activated process. The direct comparison between wrinkles,[24,36,37] moiré patterns and intercalated structures is used to confirm the intercalation process and establish a set of criteria for the assessment of molecular intercalants.

DOI: 10.1021/acs.nanolett.5b02851

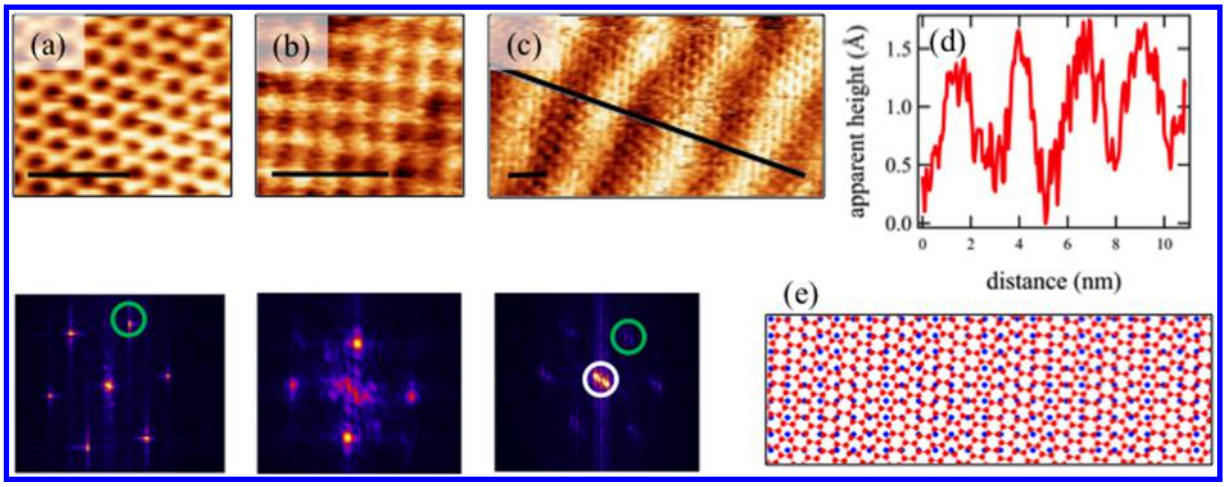

Figure 1. STM topography images of (a) graphene surface, (b) Cu(001), (c) moiré pattern with superimposed graphene honeycomb lattice, and (d) linescan along the diagonal of (c). The bottom row shows the corresponding Fourier transforms illustrating the hexagonal and square lattices, respectively. The green circles mark graphene spots, and the white circle marks the moiré pattern with its longer wavelength. (E) Geometric simulation of the moiré pattern for a 5° rotation between graphene and Cu lattice, which corresponds to the one seen in (c). The scalebar is 1 nm in all images.

This study was performed in an Omicron Variable Temperature ultrahigh vacuum scanning probe microscope with a base pressure of $<2 \times 10^{-10}$ mbar, which is connected to a preparation chamber. The graphene sample 1 (SA1) was purchased from Graphene Supermarket, and sample 2 (SA2) was grown by CVD on polycrystalline copper. The growth process for SA2 is described in ref.[38] Both sample surfaces were dominated by single layer graphene, albeit SA2 had a lower graphene coverage as deduced from STM imaging. Both samples show extended regions of Cu(100) grains, which was the focus of our work. Atomic resolution images of graphene as well as the Cu−surface were obtained for both samples. The samples were annealed prior to STM measurements and intercalation experiments to about ∼623 K for 20 min to remove adsorbates and reduce the Cu−surface. Atomically resolved STM images of the bare Cu(100)−surface[39] recorded in close proximity to graphene and intercalated structures of interest, confirm that the oxide has been removed in all areas used for study in the present manuscript. In addition, moiré patterns seen on SA1 and SA2 are commensurate with a clean Cu−graphene interface and an example is included in Figure 1. Higher annealing temperatures were avoided to minimize ripple formation caused by the different thermal expansion coefficient in Cu and graphene. Yang et al.[40] demonstrated that oxide formed on Cu by oxidation in ambient can indeed be removed completely by annealing in vacuum at 573 K, which is commensurate with our observations, whereas oxidation at higher temperatures forms a more resilient oxide. We assume that oxygen contamination in the gas phase during graphene growth can lead to a much more persistent oxide layer, and details of graphene growth on Cu-oxide have been discussed by Gottardi et al.[41]

C_{60} was deposited by thermal evaporation of high purity C_{60} powder (MerCorp) from a h-BN crucible with graphite liner. The deposition rate was measured with a quartz crystal monitor and kept constant at 1 ML/min; the C_{60} layer was deposited at room temperature and the thickness of the initial C_{60} layer was between 2 and 20 ML. The Cu−graphene−C_{60} sample was then annealed at temperatures between 573 and 753 K for 5−20 min to drive the molecules into the interfacial space and achieve intercalation. Intercalation was observed for annealing temperatures above 623 K (above the sublimation temperature of C_{60}), shorter annealing times (<10 min), and shorter ramp up-times to annealing temperature (<15 min) likewise favor intercalation over complete desorption. A shorter overall time (ramp-up plus annealing time) is favorable for the formation of an ordered (crystalline) over a disordered (amorphous) intercalate.

The initial graphene surface and each deposition step were studied with STM and STS. The sample preparation and deposition was performed in a preparation chamber, which shares the vacuum with the microscope, and the samples, therefore, were kept under UHV conditions for the entirety of the experiment. STM images were recorded in constant current mode at room temperature with electrochemically etched tungsten tips. A tunneling current of 1 nA was used for all STM images. Typically, graphene was measured with $V_{bias} = +0.085$ V for the best image quality, and the voltage was varied between 0.085 and 0.3 V for some of the intercalated structures. STS data sets were measured on graphite and Au to confirm reproducibility and reliability of the tip performance. STM and STS data were analyzed with WSxM 5.0,[42] Igor Pro 6.22, and a MatLab program was developed for analysis and visualization of STS maps.

The STS maps were measured on a grid of 103 × 103 equidistant spectra within a 512 × 512 pixel topography image. The feedback-loop was switched off for every ST spectrum, and switched on for topography imaging in between spectra. The derivative dI/dV and normalized conductance $dI/dV/(I/V)$ [differential conductance] spectra were obtained numerically using the methods described by Feenstra and Tromp.[43−45] Topography images, which were recorded simultaneously with the STS maps, were used to calculate drift between subsequent STS maps. In the analysis of the crystalline intercalated structure, we averaged over five drift-corrected STS maps measured consecutively to improve the signal-to-noise ratio.

The results section first discusses the wrinkles in graphene as an example for a free-standing graphene, and will then move on to moiré patterns between graphene and Cu(001) as examples of a superlattice imprinted on graphene. We will then introduce amorphous intercalates (where the intercalated molecules are arranged in an irregular manner) and crystalline intercalates

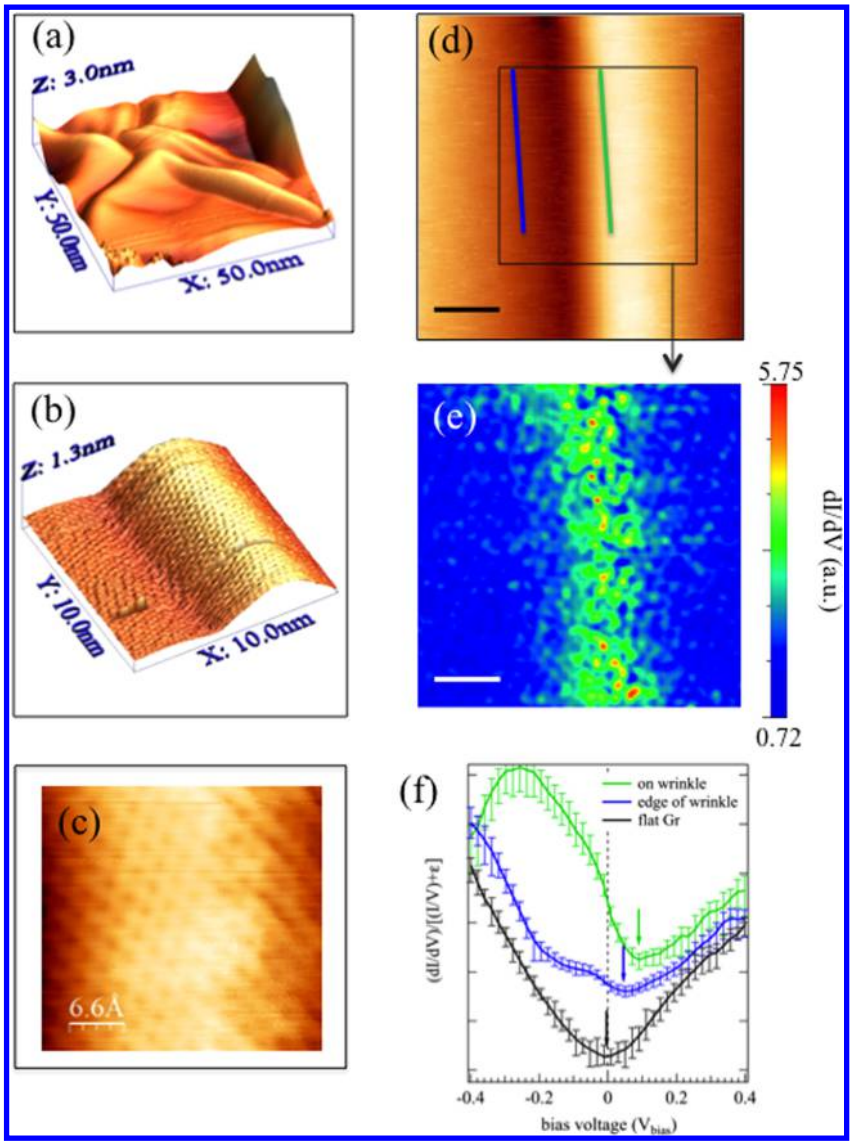

Figure 2. (a) 3D image of a four-way wrinkle in graphene, (b) 3D image of a single wrinkle with atomically resolved graphene lattice as shown in (c), which was recorded at the center of the wrinkle. (d) Top view of the same wrinkle shown in (b) (scale bar = 5 nm); the green (blue) line corresponds to the line along which the ST spectra from (f) were collected and averaged. (e) STS map for V_{bias} = 9.2 mV within the boxed area marked in (d). The wrinkle coincides with the higher dI/dV values in agreement with the spectra displayed in (f), which includes the spectra averaged along the lines indicated in (d). (f) Displays representative dI/dV spectra; the error bars indicate the variation in the spectra used for averaging: parallel to the wrinkle axis on top of the wrinkle (green), and at the edge of the wrinkle (blue). The spectrum for graphene on Cu prior to C_{60} intercalation (black) is included for comparison. The spectrum for the C_{60} layer prior to intercalation is identical to spectra shown in the literature[47,48] and has a bandgap of 2.3 eV.

(where the C_{60} molecules are arranged in a regular, square pattern) and compare the topographic and electronic structure of wrinkles, moiré pattern, and intercalated material. This comparison is used to confirm successful intercalation and it illustrates the significant variation between the structures.

Figure 2 displays the STM and STS data obtained for wrinkles, which form after sample annealing due to the mismatch of thermal expansion coefficients of graphene and Cu. Wrinkles are regions on the surface where graphene has detached from the substrate but is not folded over.[46] Figure 2a shows an example of a complex 4-fold wrinkle on SA2, and Figure 2b is a single wrinkle; both were observed after deposition of 18 molecular layers of C_{60} on SA2, and annealing at 723 K for 5 min with a ramp-up time of 15 min to drive the intercalation. The intercalate seen on other sections of this sample had an amorphous structure as discussed in the next section. The images of the wrinkles, and the atomic resolution of the honeycomb lattice (Figure 2c), confirm that the graphene is not folded in on itself. The graphene lattice is resolved across the entire wrinkle and Figure 2d–f summarize the spectroscopy data. The black square in Figure 2d is the same image section as the 3D depiction in Figure 2b, and marks the region of the STS map in Figure 2e. The map is a cut through all dI/dV spectra at 9.2 mV in the conduction band. The higher dI/dV values on the wrinkle itself are distinguished in the color-coded map by a green color, whereas blue corresponds to a lower dI/dV value characteristic of the Cu–graphene signature expected on either side of the wrinkle. The ST spectra of the fullerene layers prior to intercalation show the fullerene bandgap of 2.3 eV are identical to spectra measured

previously with STS[47] and agree with the spectra of the occupied and unoccupied electronic states of C_{60} on graphite as determined by photoemission and X-ray absorption.[48] The fullerene layer has a thickness of a few MLs and the bandgap is fully developed with E_F positioned at the center of the gap.

The corresponding differential conductance spectra are shown in Figure 2f, which includes the spectra for graphene on Cu recorded at the edge of the measurement window, graphene at the center of the wrinkle, and graphene at the boundary of the wrinkle. Each of these spectra is averaged over the area marked by the green and blue lines, respectively; the error bar indicates the variation of spectral signatures along this line. E_D is tentatively assigned to the lowest dI/dV value and is marked with an arrow. The STS for graphene on Cu is measured at the left side of the images and several nanometer removed from the wrinkle. The shape of the spectra at the edge of the fold along the blue line replicate the general shape of the graphene on Cu spectra except for a slight shift of E_D by ~0.06 eV, and superposition of several weak, step-like features.

For the spectra measured on the wrinkle, the overall shape is more strongly modified and the minimum is shifted by ~0.09 eV with respect to E_F. The number of very noisy spectra with significant signal excursions, which are unsuitable for analysis, is considerably higher for measurements on the wrinkle. Without the ability to control E_F with a gate the assignment of Dirac energies should be taken with a grain of salt.[49] However, if the tentative assignment is correct then E_D on the fold corresponds to a slight p-type doping possibly caused by the strain field in the wrinkle. The higher dI/dV values and step-like fluctuations for spectra measured on the wrinkle can be attributed to deformations of graphene during measurement.[36] The local electrostatic field around the tip exerts a force on the graphene leading to a small "dent" or a "pull" on the surface. The tunneling current will therefore be modified by contributions from the interactions with the tip side, consequently leading to variability in the spectral shape.[50] In addition to the contributions from the mechanical deformation, a modulation of the local density of states (LDOS) can contribute to the increased dI/dV to E_F, although the work by P. Xu et al.[36] indicates that the contribution from the mechanical distortion dominates. This analysis demonstrates that wrinkles in graphene are suitable model systems for free-standing graphene, and high resolution topography and spectroscopic data can be obtained.

The second type of surface structure, which is ubiquitous in the study of graphene, are moiré patterns caused by the lattice mismatch between graphene and the substrate which imprint a superlattice on graphene whose periodicity depends on the structure of the substrate and the orientation of graphene with respect to the substrate lattice.[23] The characterization of moiré patterns for graphene on Cu will be used later for comparison of corrugations observed in the intercalated structures. Moiré patterns were observed on all samples and the example in Figure 1 is from SA2. A recent publication by Gottardi et al.[41] report a selection of moiré patterns for graphene on Cu-oxides/Cu(111) surface with a similar corrugation but different periodicity compared to the ones reported here for the Cu(001) surface. Figure 1 shows atomically resolved graphene, a Cu(100) surface adjacent to this graphene island, a moiré pattern, and the corresponding Fourier transforms presented below each image. The combination of a hexagonal graphene with a square Cu(100) structure yields a striped pattern for 5° rotation, which was confirmed by using a purely geometric model with rigid lattices (see sketch next to the Fourier transform). The profile along the black line of Figure 1c reveals a corrugation across the moiré pattern of 0.15 nm with a wavelength close to 3 nm, and this value was found to be insensitive to variations in V_{bias} during imaging.

A representative example of intercalated fullerenes with an amorphous structure (SA1, T = 723 K, 5 min anneal with a 10 min ramp to temperature) is shown in Figure 3. We prepared

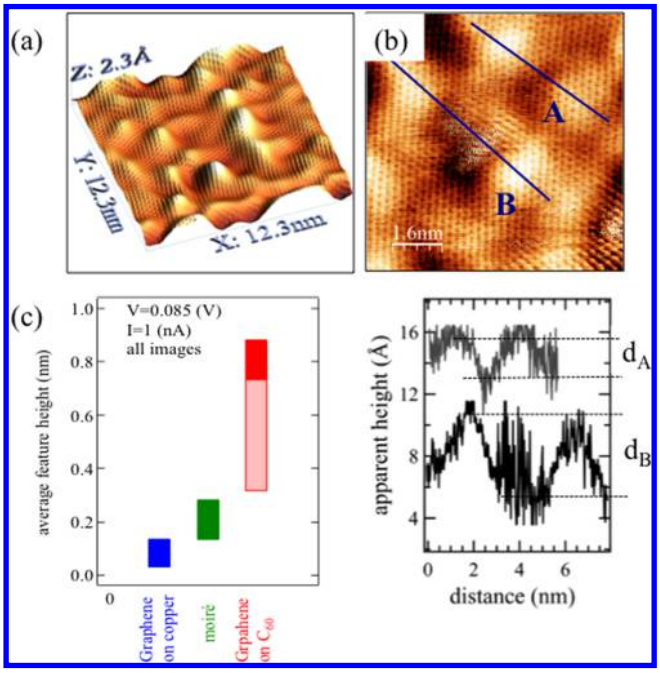

Figure 3. (a) 3D STM topography image of an amorphous intercalated structure; the graphene lattice on top of the C_{60} molecules is resolved (Note: this image was Fourier filtered to reduce noise, image b is an unfiltered 2D image of same sample). (b) Image section of the amorphous intercalated structure and two linescans are shown below the image. Molecules along line A (line B) are separated by 3 nm (4.1 nm) and d_A (d_B) in the linescans indicates the apparent height for the respective intermolecular distances. (c) Summary of average feature heights observed for graphene on Cu, moiré patterns such as the one shown in Figure 1, and the wide range of feature heights observed in the intercalated structures. Isolated fullerene molecules will have an apparent height of about 0.8 nm when buried beneath graphene.

several samples with similar conditions (see experimental section for details) and observed amorphous intercalated structures on different areas with variable molecule density. Figure 3a shows a typical STM image of the amorphous intercalated structure with intermolecular distances between 3 and 8 nm. The average diameter of the molecule shape imprinted on the graphene layer is about 1.3 nm, which is consistent for all samples and slightly larger than the C_{60} diameter of 1 nm measured for isolated molecules on a graphite surface due to "blanketing" by the graphene overlayer. Figure 3b includes several intercalated fullerene molecules, and two representative linescans marked A and B for intermolecular distances of 3.0 and 4.5 nm, respectively, are shown below the image. The feature height depends on the intermolecular distance and is defined as the magnitude of the dip between two fullerene molecules, d_A and d_B as marked in the linescans. d_A for the closer spaced molecules is considerably smaller than d_B for the larger intermolecular distance. The smaller dip is

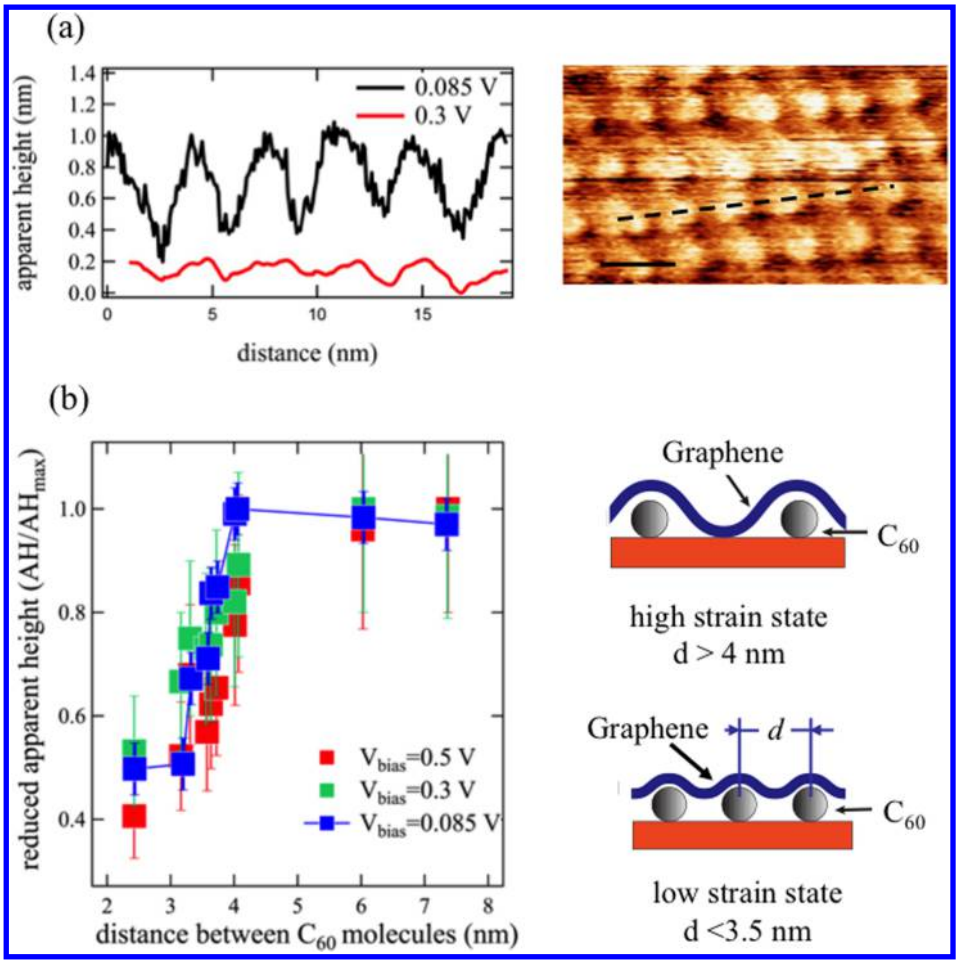

Figure 4. (a) shows a crystalline intercalated structure and a linescan for V_{bias} of 0.085 and 0.3 V of the same image section. The corresponding data points are included in (b) for 3.4 nm intermolecular distance. (b) Reduced apparent height calculated by division of the apparent height (AH) of the molecules by the maximum AH measured for the largest molecule distance at the same V_{bias}. The reduced apparent height for three bias voltages is included and they collapse onto a single step-like function. The drawing on the right-hand side visualizes the high and low strain states.

related to a detachment of graphene from the substrate in between closely spaced molecules and appears as a "ridge" in the 3D image. A comparison of the corrugation between graphene on Cu, the moiré pattern shown in Figure 1, and the range of feature heights observed in intercalated structures in Figure 3c visualizes the impact of intercalation on the deformation of the graphene layer. Graphene on top of an amorphous intercalated structure shows a significantly larger feature height, and feature height variability than any other substrate-induced corrugation.

Figures 4 and 5 present the crystalline intercalated structure prepared on SA1 [annealed at 673 K for 5 min with a 4 min ramp up to temperature]. The linescan across the crystalline intercalated structure seen in Figure 4a illustrates the significant change in apparent height as a function of bias voltage, which has been observed for all intercalated structures. The average apparent height (AH) of the intercalated fullerenes changes significantly as a function of V_{bias} for the amorphous and the crystalline intercalated structures in the same manner and the largest corrugation is observed for V_{bias} = 0.085 V. The strong variation of apparent height with bias voltage has been reported previously[51,52] for C_{60} intercalated at the Ni/graphene interface and is independent of spatial arrangement and substrate material albeit this behavior of intercalated molecules is currently not well understood.

Figure 4b summarizes the reduced AH defined by [AH at a given voltage]/[maximum AH measured for the respective bias voltage observed for intermolecular distances above 4 nm] as a function of intermolecular distance. All data for amorphous and crystalline structures (data point for 3.4 nm intermolecular distance) collapse onto a step-like function where the magnitude of the dip between the molecules depends only on the intermolecular distance. The reduced AH is 1 for fullerenes with an intermolecular distance >4.0 nm but decreases rapidly for shorter distances. A high strain state with large local deformation of graphene is achieved if the graphene layer is in contact with Cu in between the molecules, and a low strain state is seen if graphene becomes detached from the substrate and is only in contact with the molecules. The transition between the low and high strain states occurs between 3.0 and 4.0 nm, and is controlled by the interfacial energies for Cu−C_{60}, graphene−C_{60}, and Cu−graphene and by contributions from the deformation energy of graphene.[53] The detachment of graphene from the substrate is driven by its inherent stiffness with a high in-plane Young's modulus.[26,35,36,46,54,55]

The work by Yamamoto et al.[56] provides insight in the stability of wrinkles in graphene, which form in response to the presence of nanoscale particles placed between substrate and graphene. This work used SiO_2 particles with an average

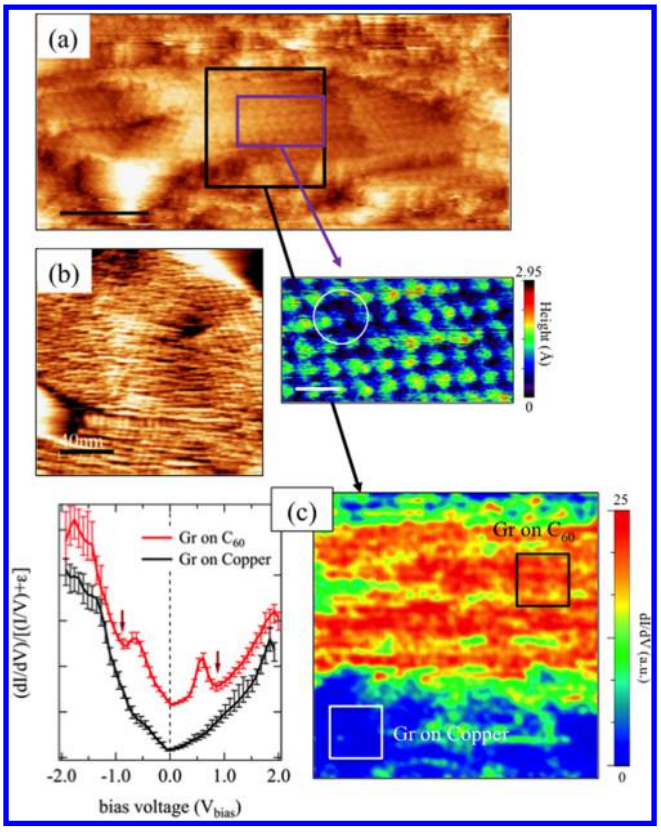

Figure 5. (a) and (b) Representative STM topography images of the crystalline intercalated structure (scale bar = 40 nm). The image region marked with a purple rectangle is enlarged and shown in a different color scheme to enhance image contrast. The white circle marks a vacancy in the intercalant lattice. (c) ST spectra from the crystalline intercalated structure (Gr on C_{60}, red) and graphene on Cu for comparison (Gr on copper, black). The arrows mark the position of the spectral minimum, most likely the Dirac energy, and the two minima associated with the superlattice peaks from the crystalline intercalated structure. The spectroscopy map at V_{bias} = 37 mV reflects the spatial distribution of the crystalline intercalation region with a higher dI/dV (red and yellow color) and includes a section with graphene on Cu at the bottom of the frame with a significantly lower dI/dV value (blue) in agreement with the spectra. The ST spectra were obtained by averaging over the area indicated by the black and white squares in the map (see text for details).

diameter of 7.5 nm—nearly an order of magnitude larger than the fullerene molecules—and a concise description of wrinkle deformations was developed. The maximum wrinkle length X_c is defined as the distance over which a wrinkle is sustained due to the rigidity of the graphene lattice and given by $X_c \sim d(E_{2D}/\Gamma)^{1/4}$. E_{2D} is the tensile rigidity with 2.12×10^2 eV/nm^2, d is the height of the deflection. The adhesion or interaction energy per unit area Γ between graphene and Cu(100) is given as 0.0826 eV/carbon atom or 3.28 eV/nm^2, respectively.[53,57] Using d = 1 nm, which is equivalent to the center-to-center intermolecular distance in the solid, and d = 0.8 nm, which is the radius of the carbon cage, the maximum wrinkle length is ~5 nm, or ~4 nm, respectively.[58,59] If the distance between the molecules is larger than the wrinkle will "sag" and graphene touches the substrate. This value is in surprisingly good agreement with our experimental values, where the graphene will contact the Cu-substrate for a wrinkle length (= intermolecular distance) of more than 4 nm. This comparison strongly indicates that the mechanical behavior of graphene can still be described within the continuum-type models used by Yamamoto et al.[56] even on length scales which are close to the C−C bond length. In summary, the graphene strain field can be manipulated on a nanometer scale by controlling the geometry of the intercalation structure.

Figure 5 showcases all aspects of the crystalline intercalated structure including topography images and differential conductance maps. Figure 5a and b show islands and extended regions covered with the square lattice, which is characteristic for the crystalline intercalated structure. These regions are observed all over the sample, and short annealing and ramp-up times favor the crystalline intercalated structure. In contrast to the imaging of the amorphous intercalated structure, atomic resolution was not achieved for the crystalline structure. The short intermolecular distance of about 3.4 nm and the small dip in AH correspond to a low strain state and the graphene layer is detached from the Cu substrate between the molecules. The graphene layer, therefore, is susceptible to motion under the influence of the tip during measurement, which prevents atomic resolution and might account for the increased magnitude of dI/dV at E_F (Figure 5c). A section in Figure 5a marked by the purple rectangle is shown separately in a different color scheme to enhance contrast: the square symmetry of the intercalated structure is apparent and it is even possible to identify a point defect: a missing molecule in the upper left-hand corner marked by a circle.

An area where graphene is in contact with Cu is located at the bottom edge of the image in Figure 5a and the corresponding ST spectra are included in Figure 5c. The good agreement with the spectroscopy signature of graphene on Cu recorded prior to intercalation confirms this assignment. The electronic structure of the crystalline intercalated material is summarized in Figure 5c which includes a spectroscopy map of the area marked by a black rectangle in (a) for V_{bias} = 0.037 V. The spectra for the intercalated structure show a minimum close to E_F albeit with a higher value of the differential conductance. The ST spectra shown in Figure 5c were obtained by averaging over the selected areas in the STS map; each segment includes about 250 individual spectra, and ~6% of the spectra were rejected due to a very poor signal-to-noise ratio. The most striking difference in the crystalline intercalated surface regions compared to graphene on Cu are two additional peaks, minima in the empty and filled states, respectively, which are symmetrically positioned at ±0.9 eV. These minima are seen in all spectra recorded in the crystalline intercalated region including those outside the marked segment.

The expression given by Yankowitz et al.[33] can be used to calculate superlattice signatures in graphene

$$E_S = \pm\frac{2\pi}{\sqrt{3}\lambda}\hbar v_F \text{ obtained by substituting } |\mathbf{G}| = \frac{4\pi}{\sqrt{3}\lambda}$$
$$\text{in } E_S = \frac{\pm\hbar v_F|\mathbf{G}|}{2}$$

with E_S as the energy of the superlattice signature, $|\mathbf{G}|$ as the reciprocal lattice vector of the superlattice, λ the wavelength of the topographic superlattice as measured from the STM images, and v_F the Fermi velocity of 1.1×10^6 m/s.[22] For the crystalline intercalated structure, the wavelength is about 3.4 nm, and yields a superlattice minimum at 0.78 eV, which is very close to the experimentally observed position at 0.9 eV. An alternative interpretation for the presence of additional peaks in the ST spectra is a resonant tunneling through the molecular energy

levels in the fullerene molecules, albeit the symmetry of the peaks (minima) with respect to E_F, and the good agreement with the above calculation supports the interpretation as superlattice peaks. This assessment strongly indicates that the fabrication of a crystalline intercalated structure leads to the formation of topographic as well as electronic superlattices defined by the local strain field, where Dirac cone replicas lead to the appearance of a superlattice peak.

The intercalation of C_{60} molecules at the graphene−Cu interfaces is confirmed using the following set of criteria:

(i) The features imprinted in graphene, which are correlated with the molecules have a diameter slightly larger than the free-standing molecule and exhibit only a small variability in diameter.

(ii) Atomic resolution of the graphene lattice is achieved if the intermolecular distances exceed about 4 nm when the graphene is still in contact with Cu. Atomic resolution can be limited by the detachment of graphene from the substrate,[54,56] which can contribute to the tip induced motion of the graphene layer

(iii) The electronic structure as expressed in the ST spectra is different from molecules residing on a graphene surface.

(iv) The corrugation of the surface is significantly larger than the corrugation observed for moiré patterns. The square symmetry of the crystalline intercalated structure cannot be achieved by moiré patterns in combination with the hexagonal graphene lattice.

(v) In addition, the height variations as a function of V_{bias} observed in the amorphous and crystalline intercalated structures are in agreement with intercalation experiments reported in the literature,[52] and these results have been reproduced for several samples, using different tips, and are not observed for other surface structures.

In combination, these observations allow us to state with confidence that molecule intercalation has been achieved, and establish general guidelines for assessing molecule intercalation processes. This is particularly important since the intercalation of a large molecule is initially counterintuitive but has been observed previously, albeit not widely reported, for C_{60} intercalation in graphite.[24,60,61]

Recent experiments, which produce localized strain fields in graphene, are microbubbles at the Pt−graphene interface, exhibiting locally a Landau level splitting equivalent to a 300 T pseudomagnetic field, nanobubbles at the Ru−graphene interface created by local oxidation and strain-driven detachment of graphene, and Pb−islands made by interacalation at the Ir−graphene interface.[13,19,34] The intercalation of C_{60} is comparable to these structures in terms of the magnitude of strain and curvature induced in graphene and is likely to provide a better long-term stability than nanobubbles, which are prone to lose their inventory of smaller molecules over time by diffusion along the interface or through the graphene membrane.[62] In our experience, the C_{60} intercalated structures are stable for up to several weeks in an ultrahigh vacuum environment. Their stability in air has not been tested and will depend on the interaction/adhesion of the graphene layer and C_{60} molecules to a substrate, which might oxidize over time. On the other hand, the strain field is defined by molecule dimensions, which do not change over time, and are identical for each intercalated molecule.

The position of E_D in pristine graphene−Cu, and the crystalline intercalated structures is close to E_F indicating that doping is not significant in either structure. The graphene−Cu interface frequently shows n-type doping of graphene, and the shift of E_D on clean Cu(111) and Cu(100) measured with electron spectroscopy has often been reported to be around −0.3 eV.[63] A recent study[64] demonstrated that short annealing of graphene on Cu(100) at moderate temperatures will not induce n-type doping, which only emerges after annealing at higher temperatures. The temperature-dependence of graphene doping is attributed to a reorganization/restructuring at the Cu(100)-graphene interface.[65] The intercalation of oxygen, and the presence of an oxygen-induced reconstruction[39,63] are both associated with a more dramatic shift of E_D by −0.6 eV, whereas graphene on Cu-oxide surfaces will effectively decouple graphene from the underlying metal.[41] Because we were able to measure a pristine Cu(100) surface adjacent to graphene islands, an electronic decoupling of graphene from a complete Cu-oxide layer is currently excluded, and the graphene−Cu interface in our work can be compared to the interfaces present during the lower temperature range annealing reported in ref 64.

The absence of significant doping in the intercalated structure is somewhat surprising considering the fact that charge transfer from all low index Cu surfaces to C_{60} is well documented,[48,66,67] however no charge transfer is observed between C_{60} and graphite, which can serve as a reasonable model system for graphene.[68] The charge density n in graphene is related to E_D by

$$n = \frac{(E_D)^2}{\pi \hbar^2 v_F}$$

If we assume that each C_{60} molecule is charged with one elementary charge q^- the charge density using the molecule distribution from the crystalline intercalated structure is $n = 1 \times 10^{14}$ cm^{-2}. This charge density corresponds to a shift in E_D = 0.35 eV, which is clearly much larger than the experimentally observed value. However, it is expected that C_{60} acts overall as an acceptor in this triple layer system.[48] The charge distribution and consequently position of E_D in the Cu−fullerene−graphene system clearly warrants a more detailed study and will be investigate in the future by integration of the intercalated structure in a device with a backgate.

A critical challenge in advancing the manipulation of graphene by molecule intercalation is the control over the formation of crystalline or amorphous structures, and ideally, the lattice constant of crystalline structures. Our work indicates that duration of the annealing process, annealing temperature, and ramp-up time to annealing temperature are decisive to achieve significant intercalation products for graphene on Cu, whereas the thickness of the initial C_{60} layer plays only a minor role. The temperature to achieve intercalation is above the sublimation temperature of C_{60} and the success of the process is influenced by the competition between intercalation and sublimation.

The intercalation process for molecules is currently not well understood, and we suggest starting by framing the discussion using the following energy balance:

$$E_{def}(G) + E_{interface}(G{-}M) < E_{interface}(C_{60}{-}G) + E_{interface}(C_{60}{-}M)$$

where $E_{def}(G)$ is the energy required to deform the graphene sheet to insert, and then to adapt to the deformation required

to accommodate the intercalated molecule. The interfacial term $E_{interface}$ describes the interaction between graphene and the metal substrate (M), which is transformed to a double-interface with C_{60}−graphene (C_{60}−G) and C_{60}−metal (C_{60}−M). Their relative contributions have to be weighted correctly, and this simple energy balance includes only interfacial interactions. Intercalation is likely to occur if the energetic cost of the combined reactions of deformation, and reduction of the Cu−graphene contact area is small compared to the gain made by formation of the C_{60}−graphene and C_{60}−Cu interfaces albeit kinetic limitations might be significant. These limitations pertain to the activation energy required to initiate intercalation by detaching the graphene edges from the Cu−surface, and include the diffusion of intercalated C_{60} at the interface. The intercalation of a C_{60} molecule cannot proceed by transition through the plane of the graphene layer for geometric reasons, but it has to start at a defect, grain boundary, or edge of a graphene flake/island or use a wrinkle as a conduit.

We hypothesize that the structure of the Cu−substrate surface influences the symmetry of the crystalline molecule structure, leading to the square symmetry. The lattice constant of the crystalline intercalated structures fluctuates by about 20% across the surface, which indicates that a well-defined epitaxial relation between molecule position and orientation is not achieved. The formation of amorphous structures, which are observed for longer annealing times and higher temperatures, on the other hand, is probably the result of a competition between deintercalation leading to desorption and motion of molecules in the interfacial space leading to a breakdown of the crystalline structure. In contrast, reports for C_{60} intercalation at the Ni(111)−graphene interface show only 1D wormlike channels along which the molecules accumulate but no extended intercalation in 2D.[51,52] Ni interacts strongly with graphene, whereas the interaction between graphene and Cu is much weaker with a larger interlayer distance promoting diffusion at the interface. The impact of the strain field imparted by the graphene deformation on the crystallinity of the intercalated structure remains at present speculative. Overall, our observations are commensurate with a relatively narrow stability region of the crystalline intercalated structure. The next step to develop a better understanding of the intercalation process, and to achieve control of the crystallography of the intercalated structure, will be to extend the present work and establish an "intercalation phase diagram", which covers a wider range of temperatures, annealing times, substrate materials, and substrate crystallography.

The intercalation of molecules at the Cu−graphene interface is a unique and, versatile approach to the manipulation of graphene. Considering the large size of the fullerene molecule, it seems likely that other molecules can be intercalated although for a reliable prediction of the feasibility of intercalation a better understanding of the process has to be achieved. Specifically, the intercalation of the relatively large C_{60} molecule leads to the formation of amorphous or crystalline strain lattices where the intermolecular distance tunes the magnitude of the strain state. The intercalation of molecules is a complex process, where the mutual interactions between graphene, substrate, and intercalant as well as the mechanical deformation in graphene have to be considered. A full understanding of the intercalation process needs to be achieved to fully exploit molecule intercalation as a means to adapt graphene properties and reach the desired charge carrier transport characteristics to tailor device performance in the future. Our work has shown the feasibility and richness of molecule intercalation structures and opens the path to build a wide range of materials.

AUTHOR INFORMATION

Corresponding Author

*E-mail: pr6e@virginia.edu.

Present Address

(L.B.) Elettra Sincrotrone Trieste, Area Science Park, 34149 Basovizza, Trieste, Italy.

Notes

The authors declare no competing financial interest.

ACKNOWLEDGMENTS

This work by E. Monazami and P. Reinke was supported by NSF-Division of Materials Research (Ceramics) DMR-1005809. Petra Rudolf and Luca Bignardi acknowledge the financial support by the "Graphene-based electronics" research program of the Foundation for Fundamental Research on Matter (FOM); FOM is part of The Netherlands Organization for Scientific Research (NWO).

REFERENCES

(1) Castro Neto, A. H.; Peres, N. M. R.; Novoselov, K. S.; Geim, A. K. The electronic properties of graphene. *Rev. Mod. Phys.* **2009**, *81*, 109−162.

(2) Andrei, E. Y.; Li, G.; Du, X. Electronic properties of graphene: a perspective from scanning tunneling microscopy and magnetotransport. *Rep. Prog. Phys.* **2012**, *75*, 056501.

(3) Das Sarma, S.; Adam, S.; Hwang, E. H.; Rossi, E. Electronic transport in two-dimensional graphene. *Rev. Mod. Phys.* **2011**, *83*, 407−470.

(4) Britnell, L.; Gorbachev, R. V.; Jalil, R.; Belle, B. D.; Schedin, F.; Mishchenko, A.; Georgiou, T.; Katsnelson, M. I.; Eaves, L.; Morozov, S. V.; Peres, N. M.; Leist, J.; Geim, A. K.; Novoselov, K. S.; Ponomarenko, L. A. Field-effect tunneling transistor based on vertical graphene heterostructures. *Science* **2012**, *335*, 947−950.

(5) Giovannetti, G.; Khomyakov, P.; Brocks, G.; Karpan, V.; van den Brink, J.; Kelly, P. Doping Graphene with Metal Contacts. *Phys. Rev. Lett.* **2008**, *101*, 026803.

(6) Gyamfi, M.; Eelbo, T.; Waśniowska, M.; Wehling, T. O.; Forti, S.; Starke, U.; Lichtenstein, A. I.; Katsnelson, M. I.; Wiesendanger, R. Orbital selective coupling between Ni adatoms and graphene Dirac electrons. *Phys. Rev. B: Condens. Matter Mater. Phys.* **2012**, *85*, 161406.

(7) Jeong, H. M.; Lee, J. W.; Shin, W. H.; Choi, Y. J.; Shin, H. J.; Kang, J. K.; Choi, J. W. Nitrogen-doped graphene for high-performance ultracapacitors and the importance of nitrogen-doped sites at basal planes. *Nano Lett.* **2011**, *11*, 2472−2477.

(8) Lauffer, P.; Emtsev, K. V.; Graupner, R.; Seyller, T.; Ley, L. Molecular and electronic structure of PTCDA on bilayer graphene on SiC(0001) studied with scanning tunneling microscopy. *Phys. Status Solidi B* **2008**, *245*, 2064−2067.

(9) Low, T.; Guinea, F.; Katsnelson, M. I. Gaps tunable by electrostatic gates in strained graphene. *Phys. Rev. B: Condens. Matter Mater. Phys.* **2011**, *83*, 195436.

(10) Park, J. U.; Nam, S.; Lee, M. S.; Lieber, C. M. Synthesis of monolithic graphene-graphite integrated electronics. *Nat. Mater.* **2011**, *11*, 120−125.

(11) Petrovic, M.; Srut Rakic, I.; Runte, S.; Busse, C.; Sadowski, J. T.; Lazic, P.; Pletikosic, I.; Pan, Z. H.; Milun, M.; Pervan, P.; Atodiresei, N.; Brako, R.; Sokcevic, D.; Valla, T.; Michely, T.; Kralj, M. The mechanism of caesium intercalation of graphene. *Nat. Commun.* **2013**, *4*, 2772.

(12) Pollard, A. J.; Perkins, E. W.; Smith, N. A.; Saywell, A.; Goretzki, G.; Phillips, A. G.; Argent, S. P.; Sachdev, H.; Muller, F.; Hufner, S.; Gsell, S.; Fischer, M.; Schreck, M.; Osterwalder, J.; Greber, T.; Berner, S.; Champness, N. R.; Beton, P. H. Supramolecular assemblies formed

on an epitaxial graphene superstructure. *Angew. Chem., Int. Ed.* **2010**, *49*, 1794−1799.
(13) Sicot, M.; Leicht, P.; Zusan, A.; Bouvron, S.; Zander, O.; Weser, M.; Dedkov, Y. S.; Horn, K.; Fonin, M. Size-selected epitaxial nanoislands underneath graphene moire on Rh(111). *ACS Nano* **2012**, *6*, 151−158.
(14) Silien, C.; Pradhan, N.; Ho, W.; Thiry, P. Influence of adsorbate-substrate interaction on the local electronic structure of C60 studied by low-temperature STM. *Phys. Rev. B: Condens. Matter Mater. Phys.* **2004**, *69*, 115343.
(15) Tadich, A.; Edmonds, M. T.; Ley, L.; Fromm, F.; Smets, Y.; Mazej, Z.; Riley, J.; Pakes, C. I.; Seyller, T.; Wanke, M. Tuning the charge carriers in epitaxial graphene on SiC(0001) from electron to hole via molecular doping with C60F48. *Appl. Phys. Lett.* **2013**, *102*, 241601.
(16) Zan, R.; Bangert, U.; Ramasse, Q.; Novoselov, K. S. Evolution of gold nanostructures on graphene. *Small* **2011**, *7*, 2868−2872.
(17) Zhang, Y.; Brar, V. W.; Girit, C.; Zettl, A.; Crommie, M. F. Origin of spatial charge inhomogeneity in graphene″, Nat. *Nat. Phys.* **2009**, *5*, 722−726.
(18) Pereira, V.; Castro Neto, A. Strain Engineering of Graphene's Electronic Structure. *Phys. Rev. Lett.* **2009**, *103*, 046801.
(19) Qi, Z.; Kitt, A. L.; Park, H. S.; Pereira, V. M.; Campbell, D. K.; Castro Neto, A. H. Pseudomagnetic fields in graphene nanobubbles of constrained geometry: A molecular dynamics study. *Phys. Rev. B: Condens. Matter Mater. Phys.* **2014**, *90*, 125419.
(20) Varykhalov, A.; Sanches-Barriga, J.; Shikin, A. M.; Biswas, C.; Vescovo, E.; Rybkin, A.; Marchenko, D.; Rader, O. Electronic and magnetic properties of quasifreestanding graphene on Ni. *Phys. Rev. Lett.* **2008**, *101*, 157601.
(21) Gierz, I.; Suzuki, T.; Weitz, R. T.; Lee, D. S.; Krauss, B.; Riedl, C.; Starke, U.; Hoechst, H.; Smet, J. H.; Ast, C. R.; Kern, K. Electronic coupling of an epitaxial graphene monolayer by gold intercalation. *Phys. Rev. B: Condens. Matter Mater. Phys.* **2010**, *81*, 235408.
(22) Xue, J.; Sanchez-Yamagishi, J.; Bulmash, D.; Jacquod, P.; Deshpande, A.; Watanabe, K.; Taniguchi, T.; Jarillo-Herrero, P.; LeRoy, B. J. Scanning tunnelling microscopy and spectroscopy of ultra-flat graphene on hexagonal boron nitride. *Nat. Mater.* **2011**, *10*, 282−285.
(23) Ponomarenko, L. A.; Gorbachev, R. V.; Yu, G. L.; Elias, D. C.; Jalil, R.; Patel, A. A.; Mishchenko, A.; Mayorov, A. S.; Woods, C. R.; Wallbank, J. R.; Mucha-Kruczynski, M.; Piot, B. A.; Potemski, M.; Grigorieva, I. V.; Novoselov, K. S.; Guinea, F.; Fal'ko, V. I.; Geim, A. K. Cloning of Dirac fermions in graphene superlattices. *Nature* **2013**, *497*, 594−597.
(24) Kim, K.; Lee, Z.; Malone, B. D.; Chan, K. T.; Alemán, B.; Regan, W.; Gannett, W.; Crommie, M. F.; Cohen, M. L.; Zettl, A. Multiply folded graphene. *Phys. Rev. B: Condens. Matter Mater. Phys.* **2011**, *83*, 245433.
(25) Ye, J.; Craciun, M. F.; Koshino, M.; Russo, S.; Inoue, S.; Yuan, H.; Shimotani, H.; Morpurgo, A. F.; Iwasa, Y. Accessing the transport properties of graphene and its multilayers at high carrier density. *Proc. Natl. Acad. Sci. U. S. A.* **2011**, *108*, 13002−13006.
(26) Lee, J. K.; Yamazaki, S.; Yun, H.; Park, J.; Kennedy, G. P.; Kim, G. T.; Pietzsch, O.; Wiesendanger, R.; Lee, S.; Hong, S.; Dettlaff-Weglikowska, U.; Roth, S. Modification of electrical properties of graphene by substrate-induced nanomodulation. *Nano Lett.* **2013**, *13*, 3494−3500.
(27) Calleja, F.; Ochoa, H.; Garnica, M.; Barja, S.; Navarro, J. J.; Black, A.; Otrokov, M. M.; Chulkov, E. V.; Arnau, A.; Vázquez de Parga, A. L.; Guinea, F.; Miranda, R. Spatial variation of a giant spin−orbit effect induces electron confinement in graphene on Pb islands. *Nat. Phys.* **2014**, *11*, 43−47.
(28) Guinea, F. Strain engineering in graphene. *Solid State Commun.* **2012**, *152*, 1437−1441.
(29) Guinea, F.; Katsnelson, M.; Vozmediano, M. Midgap states and charge inhomogeneities in corrugated graphene. *Phys. Rev. B: Condens. Matter Mater. Phys.* **2008**, *77*, 075422.
(30) Guinea, F.; Katsnelson, M. I.; Geim, A. K. Energy gaps and a zero-field quantum Hall effect in graphene by strain engineering. *Nat. Phys.* **2010**, *6*, 30−33.
(31) Isacsson, A.; Jonsson, L.; Kinaret, J.; Jonson, M. Electronic superlattices in corrugated graphene. *Phys. Rev. B: Condens. Matter Mater. Phys.* **2008**, *77*, 035423.
(32) Katsnelson, M. I.; Novoselov, K. S.; Geim, A. K. Chiral tunnelling and the Klein paradox in graphene. *Nat. Phys.* **2006**, *2*, 620−625.
(33) Yankowitz, M.; Xue, J.; Cormode, D.; Sanchez-Yamagishi, J. D.; Watanabe, K.; Taniguchi, T.; Jarillo-Herrero, P.; Jacquod, P.; LeRoy, B. J. Emergence of superlattice Dirac points in graphene on hexagonal boron nitride. *Nat. Phys.* **2012**, *8*, 382−386.
(34) Lu, J.; Neto, A. H.; Loh, K. P. Transforming Moire blisters into geometric graphene nano-bubbles. *Nat. Commun.* **2012**, *3*, 823.
(35) Bai, K.-K.; Zhou, Y.; Zheng, H.; Meng, L.; Peng, H.; Liu, Z.; Nie, J.-C.; He, L. Creating One-Dimensional Nanoscale Periodic Ripples in a Continuous Mosaic Graphene Monolayer. *Phys. Rev. Lett.* **2014**, *113*, 086102.
(36) Xu, P.; Yang, Y.; Barber, S. D.; Ackerman, M. L.; Schoelz, J. K.; Qi, D.; Kornev, I. A.; Dong, L.; Bellaiche, L.; Barraza-Lopez, S.; Thibado, P. M. Atomic control of strain in freestanding graphene. *Phys. Rev. B: Condens. Matter Mater. Phys.* **2012**, *85*, 121406.
(37) Li, X.; Cai, W.; An, J.; Kim, S.; Nah, J.; Yang, D.; Piner, R.; Velamakanni, A.; Jung, I.; Tutuc, E.; Banerjee, S. K.; Colombo, L.; Ruoff, R. S. Large-area synthesis of high-quality and uniform graphene films on Copper foils. *Science* **2009**, *324*, 1312−1314.
(38) Bignardi, L.; van Dorp, W. F.; Gottardi, S.; Ivashenko, O.; Dudin, P.; Barinov, A. V.; de Hosson, J. T. M.; Stoehr, M.; Rudolf, P. Microscopic characterization of suspended graphene grown by chemical vapour deposition. *Nanoscale* **2013**, *5*, 9057−9061.
(39) Jensen, F.; Besenbacher, F.; Laegsgaard, E.; Stensgaard, I. Dynamics of oxygen-induced reconstruction of Cu(100) studied by scanning tunneling microscopy. *Phys. Rev. B: Condens. Matter Mater. Phys.* **1990**, *42*, 9206−9209.
(40) Yang, J. C.; Yeadon, M.; Olynick, D.; Gibson, J. M. Anomalous desorption of Copper oxide observed by in situ transmission electron microscopy. *Microsc. Microanal.* **1997**, *3*, 121−125.
(41) Gottardi, S.; Mueller, K.; Bignardi, L.; Moreno-Lopez, J. C.; Pham, T. A.; Ivashenko, O.; Yablonskikh, M.; Bjoerk, J.; Rudolf, P.; Stoehr, M.; Barinov, A. Comparing graphene growth on Cu(111) versus oxidized Cu(111). *Nano Lett.* **2015**, *15*, 917−922.
(42) Horcas, I.; Fernandez, R.; Gomez-Rodriguez, J. M.; Colchero, J.; Gomez-Herrero, J.; Baro, A. M. WSXM: A software for scanning probe microscopy and a tool for nanotechnology. *Rev. Sci. Instrum.* **2007**, *78*, 013705.
(43) Feenstra, R. M.; Lee, J. Y.; Kang, M. H.; Meyer, G.; Rieder, K. H. Band gap of the Ge(111)c(2 × 8) surface by scanning tunneling spectroscopy. *Phys. Rev. B* **2006**, *73*, 035310.
(44) Tromp, R. M. Spectroscopy with the scanning tunnelling microscope: a critical review. *J. Phys.: Condens. Matter* **1989**, *1*, 10211−10228.
(45) Feenstra, R. M. A prospective: Quantitative scanning tunneling spectroscopy of semiconductor surfaces. *Surf. Sci.* **2009**, *603*, 2841−2844.
(46) Kim, K.; Lee, Z.; Malone, B. D.; Chan, K. T.; Aleman, B.; Regan, W.; Gannett, W.; Crommie, M. F.; Cohen, M. L.; Zettl, A. Multiply folded graphene. *Phys. Rev. B: Condens. Matter Mater. Phys.* **2011**, *83*, 245433.
(47) McClimon, J. B.; Monazami, E.; reinke, P. Interaction of C_{60} with tungsten: modulation of morphology and electronic structure on the molecular length scale. *J. Phys. Chem. C* **2014**, *118*, 24479.
(48) Rudolf, P.; Golden, M. S.; Bruehwiler, P. A. Studies of fullerenes by the excitation, emission and scattering of electrons″, *J. J. Electron Spectrosc. Relat. Phenom.* **1999**, *100*, 409−433.
(49) Zhang, Y.; Brar, V. W.; Wang, F.; Girit, C.; Yayon, Y.; Panlasigui, M.; Zettl, A.; Crommie, M. F. Giant phonon-induced conductance in scanning tunnelling spectroscopy of gate-tunable graphene. *Nat. Phys.* **2008**, *4*, 627−630.

(50) Gao, L.; Guest, J. R.; Guisinger, N. P. Epitaxial graphene on Cu(111). *Nano Lett.* **2010**, *10*, 3512−3516.
(51) Lu, J.; Zheng, Y.; Sorkin, A.; Loh, K. P. Growing suspended graphene on C60 molecules. *Small* **2012**, *8*, 3728−3732.
(52) Varykhalov, A.; Gudat, W.; Rader, O. Imaging buried molecules: fullerenes under graphene. *Adv. Mater.* **2010**, *22*, 3307−3310.
(53) Lee, C.; Wei, X.; Kysar, J. W.; Hone, J. Measurement of the elastic properties and intrinsic strength of monolayer graphene. *Science* **2008**, *321*, 385−388.
(54) Kushima, A.; Qian, X.; Zhao, P.; Zhang, S.; Li, J. Ripplocations in van der waals layers. *Nano Lett.* **2015**, *15*, 1302−1308.
(55) Lu, J.; Bao, Y.; Su, C. L.; Loh, K. P. Properties of strained structures and topological defects in graphene. *ACS Nano* **2013**, *7*, 8350−8357.
(56) Yamamoto, M.; Pierre-Louis, O.; Huang, J.; Fuhrer, M. S.; Einstein, T. L.; Cullen, W. G. "The Princess and the Pea" at the nanoscale: wrinkling and delamination of graphene on nanoparticles. *Phys. Rev. X* **2012**, *2*, 041018.
(57) Klaver, T. P. C.; Zhu, S.-E.; Sluiter, M. H. F.; Janssen, G. C. A. M. Molecular dynamics simulation of graphene on Cu(100) and Cu(111) surfaces. *Carbon* **2015**, *82*, 538−547.
(58) Goel, A.; Howard, J. B.; Vander Sande, J. B. Size analysis of single fullerene molecules by electron microscopy. *Carbon* **2004**, *42*, 1907−1915.
(59) Zhou, O.; Fischer, J. E.; Coustel, N.; Kycia, S.; Zhu, Q.; McGhie, A. R.; Romanow, W. J.; McCauley, J. P.; Smith, A. B.; Cox, D. E. Structure and bonding in alkali-metal-doped C_{60}. *Nature* **1191**, *351*, 462.
(60) Fuhrer, M. S.; Hou, J. G.; Xiang, X.-D.; Zettl, A. C60 intercalated graphite: predictions and experiments. *Solid State Commun.* **1994**, *90*, 357−360.
(61) Gupta, V.; Scharff, P.; Risch, K.; Romanus, H.; Müller, R. Synthesis of C60 intercalated graphite. *Solid State Commun.* **2004**, *131*, 153−155.
(62) Nair, R. R.; Wu, H. A.; Jayaram, P. N.; Grigorieva, I. V.; Geim, A. K. Unimpeded Permeation of Water Through Helium-Leak−Tight Graphene-Based Membranes. *Science* **2012**, *335*, 442−444.
(63) Walter, A. L.; Nie, S.; Bostwick, A.; Kim, K. S.; Moreschini, L.; Chang, Y. J.; Innocenti, D.; Horn, K.; McCarty, K.; Rotenberg, E. Electronic structure of graphene on single-crystal copper substrates. *Phys. Rev. B: Condens. Matter Mater. Phys.* **2011**, *84*, 195443.
(64) Marsden, A. J.; Asensio, M.-C.; Avila, J.; Dudin, P.; Barinov, A.; Moras, P.; Sheverdyaeva, P. M.; White, T. W.; Maskery, I.; Costantini, G.; Wilson, N. R.; Bell, G. R. Is graphene on copper doped? *Phys. Status Solidi RRL* **2013**, *7*, 643−646.
(65) Tian, J.; Cao, H.; Wu, W.; Yu, Q.; Guisinger, N. P.; Chen, Y. P. Graphene induced surface reconstruction of Cu. *Nano Lett.* **2012**, *12*, 3893−3899.
(66) Schull, G.; Neel, M.; Becker, M.; Kroeger, J.; Berndt, R. Spatially resolved conductance of oriented C_{60}. *New J. Phys.* **2008**, *10*, 065012.
(67) Rowe, J. E.; Rudolf, P.; Tjeng, L. H.; Malic, R. A.; Meigs, G.; Chen, C. T.; Chen, J.; Plummer, E. W. Synchrotron radiation and low energy electron diffraction studies of ultrathin C_{60} films deposited on Cu(100), Cu(111) and Cu(110). *Int. J. Mod. Phys. B* **1992**, *6*, 3909−3913.
(68) Reinke, P.; Feldermann, H.; Oelhafen, P. C_{60} bonding to graphite and boron nitride surfaces. *J. Chem. Phys.* **2003**, *119*, 12547−12552.